Charge transport in carbon nanotubes: quantum effects of electron–phonon coupling

2007 J. Phys.: Condens. Matter 19 183203

(http://iopscience.iop.org/0953-8984/19/18/183203)

IOP PUBLISHING JOURNAL OF PHYSICS: CONDENSED MATTER

J. Phys.: Condens. Matter **19** (2007) 183203 (21pp) doi:10.1088/0953-8984/19/18/183203

TOPICAL REVIEW

Charge transport in carbon nanotubes: quantum effects of electron–phonon coupling

Stephan Roche[1,4], **Jie Jiang**[2], **Luis E F Foa Torres**[1,3] **and Riichiro Saito**[2]

[1] CEA/DSM/DRFMC/SPSMS/GT, 17 avenue des Martyrs, 38054 Grenoble, France
[2] Department of Physics, Tohoku University and CREST-JST, Sendai 980-8578, Japan
[3] CEA-Léti-MINATEC, 17 rue des Martyrs, 38054 Grenoble, France

E-mail: stephan.roche@cea.fr

Received 16 October 2006
Published 4 April 2007
Online at stacks.iop.org/JPhysCM/19/183203

Abstract

This review deals with the role of electron–phonon (e–ph) coupling in quantum transport of carbon nanotubes. First, the case of low-energy phonons and weak localization phenomena is addressed, followed by a summary of inelastic scattering lengths within the Fermi golden rule. A second part outlines the contribution of high-energy optic phonon modes, and discusses the applicability limits of semi-classical transport theory. The computational methodologies used to deepen the phonon-induced dephasing or inelastic transmission range from the time-dependent Schrödinger equation and Kubo framework to a novel many-body treatment of e–ph interaction.

(Some figures in this article are in colour only in the electronic version)

Contents

[4] Author to whom any correspondence should be addressed. Current address: Center for High Performance Simulation and Department of Physics, North Carolina State University, Raleigh, North Carolina 27695-7518, USA.

1. Introduction

Carbon nanotubes (CNTs) are fascinating low-dimensional objects that offer an outstanding playground to challenge the quantum theory at the nanoscale, manifesting novel physical phenomena. Amongst a wealth of eminent properties, electronic transport stands as a driving force to scientific excitement and technological innovation [1, 2] in CNTs.

Single-walled metallic carbon nanotubes (SWNTs) behave as long ballistic conductors [3] owing to the reduced backscattering from elastic disorder (vacancies, topological defects,...) [4]. Within the Fermi golden rule (FGR), the estimated elastic mean free paths usually reach several micrometres if the Fermi level is located close enough to the charge neutrality point (CNP). This property has been confirmed experimentally when measuring the conductance of small-diameter metallic tubes contacted to palladium electrodes [5]. Semiconducting nanotubes have been consequently used to engineer ballistic field effect transistors (CNT-FETs) [6, 7].

Ballistic transport is however limited to the low-bias regime, for which propagating electrons can only be coupled to low-energy acoustic phonon modes [8]. By increasing the potential bias across the nanotube, the contribution of electron–phonon mediated backscattering is assumed to be steadily enhanced until a saturation regime is reached in the I–V characteristics of metallic tubes [9–11]. This not only brings serious performance limitations in the current-carrying capacity of CNTs, but also raises fundamental questions about the nature of inelastic quantum transport in these unique objects [12–19].

In the high-bias regime, on the basis of semiclassical transport description, the inelastic scattering lengths are usually estimated to be in the order of a few tens of nanometres. Experimentally, Park and co-workers [10] have proposed some quantitative estimation of inelastic mean free paths (ℓ_{ie}) in both low-bias and high-bias regimes, on the basis of a phenomenological law between the measured conductance and ℓ_{ie}, namely

$$G \sim \frac{2e^2}{h}\frac{\ell_{\mathrm{ie}}}{L_{\mathrm{tube}}}. \tag{1}$$

At low bias, their data indicate that $\ell_{\mathrm{ie}} \simeq 1.6\ \mu$m, which has been attributed to acoustic modes (ℓ_{ac}), whereas for bias voltage of the order of 1 V $\ell_{\mathrm{ie}} \simeq 10$ nm has been assigned to optic (ℓ_{opt}) and/or zone-boundary phonons (ℓ_{zb}). Other estimations obtained by fitting of the experimental data with semi-classical Monte Carlo models [5] lead to typical values $\ell_{\mathrm{ac}} \simeq 300$ nm and $\ell_{\mathrm{opt}} \simeq 15$ nm for acoustic and optic modes respectively. On the other hand, within the framework of effective mass formula and deformation potential approximation [8, 10], a crude theoretical estimation of the electron–acoustic phonon scattering length yields $\ell_{\mathrm{ac}} \simeq 2.4\ \mu$m in the low-bias regime, whereas $\ell_{\mathrm{opt}} \simeq 180$ nm and $\ell_{\mathrm{zb}} \simeq 37$ nm were obtained in the high-bias regime. By applying a Mathiessen rule, a total scattering length of 30 nm was inferred. To reconcile theory with experiment a hot phonon scenario was proposed in [13]. The discussion is not yet settled [11, 19] and many questions regarding the nature of e–ph interaction in these systems remain open: What is the ultimate mechanism leading to current saturation? Is it within the reach of a semiclassical description of transport? If a hot phonon scenario is in place, can we rely on a perturbative scheme to provide answers in such an out-of-equilibrium situation?

In addition to the above-mentioned studies, e–ph coupling in carbon nanotubes has been intensively investigated theoretically in relation with temperature-dependent resistivity in metallic carbon nanotubes [24], excited-state carrier lifetime [25–27], excitonic physics [28], temperature dependence of the band gap of semiconducting nanotubes [29], superconductivity [30], and phonon-assisted tunnelling in the Coulomb blockade regime [31].

The impact of e–ph coupling on the physical properties of carbon nanotubes is thus of broad and prime importance in deepening the exceptional physical properties of CNTs.

In this review article, we focus on quantum transport through CNTs in the presence of e–ph interaction. Rather than giving an extensive review of the whole literature in this rapidly evolving field, we concentrate on some recent developments that go beyond semiclassical transport theories (Boltzmann equation). In section 2, we start by presenting a time-dependent one-body description of electronic motion in the presence of lattice vibrations. A scheme to solve the associated time-dependent Schrödinger equation as well as quantum transport in the Kubo framework is developed [15]. By using this scheme, the role of low-energy phonons in weak localization phenomena is discussed in section 3. Section 4 deals with the calculation of e–ph scattering rates within the Fermi golden rule. Recent experimental results on the current-carrying capacity in metallic nanotubes are briefly outlined in section 5, followed by a discussion of the role of high-energy phonons in section 6. Section 7 provides a novel perspective based on a many-body description of e–ph interaction [32, 33].

2. Vibration-mediated time-dependent Hamiltonian and Kubo framework

To investigate the quantum dephasing and decoherence of electronic transport in carbon nanotubes, owing to the coupling of electrons to the vibrational modes, some of us have recently proposed a new numerical approach which consists in computing the time-dependent quantum dynamics of electronic wavepackets (for π-electrons), under the action of a time-dependent Hamiltonian that mimics the atomic distortions in real space, as well as the strength of e–ph coupling [15]. For selected phonon modes (acoustic or optic), the time-dependent Schrödinger equation (TDSE) is solved by splitting the total elapsed time into finite intervals during which the energetics is given by a frozen Hamiltonian. Then, within the Kubo formalism and framework, the conductance scaling can be studied and, for low-energy electrons, the energy-dependent coherence length scaling can be extracted from the conventional weak localization phenomenology [34]. In this section, we present the energetics of the system, while the discussion on the effects of inelastic scattering on weak localization is deferred to the next section.

The real space resolution of the TDSE is achieved as follows [36]. The initial starting Hamiltonian is the π-effective model:

$$\hat{\mathcal{H}}_{\text{eff}} = \sum_i \varepsilon_i |\pi_i\rangle\langle\pi_i| + \sum_{i,\delta=1,3} \gamma(r_{i,i+\delta})(|\pi_i\rangle\langle\pi_{i+\delta}| + \text{h.c.}), \tag{2}$$

where onsite energies are either all set to zero in the absence of elastic disorder, or taken at random within the interval $[-W/2, W/2]$, when simulating an elastic disorder (Anderson-type disorder). The overlap integrals between $|\pi_i\rangle$ and $|\pi_{i+\delta}\rangle$ orbitals are restricted to first neighbours and are given by $\gamma_{i,i+\delta} = \gamma_0$ for all pairs in the case with zero phonons. The effect of phonon vibrations and e–ph couplings is further included by assuming that propagating wavepackets will suffer from a time-dependent change of the electronic energetics ($\gamma_{i,i+\delta}$-matrix) of the underlying effective Hamiltonian. In a weakly disordered two-dimensional (2D) system, similar treatment of time-dependent perturbation in the weak localization regime has been shown to correctly reproduce frequency-dependent conductivity corrections [38].

The e–ph interaction is thus encoded through the time-dependent modulation of the hopping interaction, that is $\gamma_0 \to \gamma(r_{i,i+\delta})$, where $r_{i,i+\delta}$ is the bond length. The bond-length-dependent Hamiltonian matrix elements γ are calculated by using the analytical expression given by Porezag *et al* [39], that is

$$\gamma(r_{i,i+\delta}) = \gamma(\hat{\delta} \cdot (\mathbf{R}_{i+\delta}(t) - \mathbf{R}_i(t))), \tag{3}$$

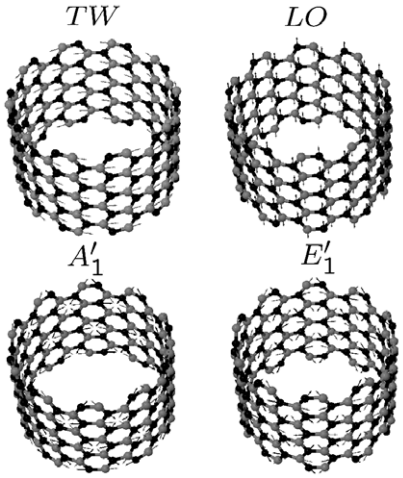

Figure 1. Representation of phonon polarization vectors for the twist mode (TW) at $q = 0$, together with longitudinal optic (LO) and zone-boundary modes A_1' and E_1'.

where the C–C bond length is $r_{i,i+\delta} = \hat{\delta} \cdot (\mathbf{R}_{i+\delta} - \mathbf{R}_i)$, with $\hat{\delta}$ the bond direction. The atomic positions for a given phonon mode with wavevector $\mathbf{q}$ and frequency $\omega_\nu(\mathbf{q})$ are given by [15]

$$\mathbf{R}_i = \mathbf{R}_i^0 + A_\nu(\mathbf{q})\mathbf{e}_\nu(\mathbf{q}) \cos(\mathbf{q} \cdot \mathbf{R}_i^0 + \omega_\nu(\mathbf{q})t), \tag{4}$$

where $\mathbf{R}_i^0$ are the equilibrium atomic positions, while A, $\mathbf{e}$ and ω are the phonon amplitude, eigenvector and frequency, respectively. As usual, the phonon amplitude can be expressed by [40]

$$A_\nu(\mathbf{q}) = \sqrt{\frac{\hbar n_\nu(\mathbf{q})}{2m_c\omega_\nu(\mathbf{q})}}. \tag{5}$$

Here m_c is the atomic carbon mass, while $n_\nu(\mathbf{q})$ is the phonon occupation number for phonon branch ν, as a function of phonon wavevector $\mathbf{q}$. For thermal equilibrium, if $n_\nu(\mathbf{q}) = 1/(e^{\hbar\beta\omega_\nu(\mathbf{q})} - 1)$ is the Bose–Einstein occupation factor, $\beta = k_B T$ and $\hbar\omega_\nu(\mathbf{q})$ is the phonon energy.

The phonon dispersion relations and eigenvectors are computed from the dynamical matrix in an SWNT [1]. Due to the C_N symmetry of the SWNT, the $6N \times 6N$ dynamical matrix is decoupled to N 6×6 matrices (N is the number of hexagons in a nanotube unit cell) [25]. We then work within the graphene unit cell, which has only one (A, B) atom pair. In the calculations, the z axis is chosen along the tube axis, while the x axis passes through the A atom in the graphene unit cell.

The important phonon modes in the transport of metallic nanotubes are twisting (TW), longitudinal optic (LO), A_1', and E_1' modes, whose frequencies are respectively 0, 1596, 1369, and 545 cm^{-1}. The symmetries of these modes are shown in figure 1 for illustration.

The phonon polarization vector plays an important role in the e–ph coupling. Amongst the zone-centre phonon modes, the LO mode is the one that could most efficiently contribute to inelastic backscattering, whereas among the boundary phonon modes, the dominating contribution is expected to come from the A_1' mode [8, 10]. Concerning the TW mode, the two atoms of the unit cell move along the same direction along the tube circumference (see figure 1). In contrast, for the LO mode, the two atoms of the unit cell move one against the other along the z axis (see figure 1). For the A_1' mode, the six atoms on a hexagon move

towards or away from the centre of the hexagon (see figure 1), whereas for E_1' mode with higher frequency, the tube vibrates, like pulling the tube at the two ends.

In our model, however, absorption and emission are both assumed to be related to a given amplitude A_0 for a initially thermalized phonon occupation at room temperature, for both LO and A_1' modes. However, it has been recently pointed out that such a hypothesis might not be valid during high-field electron transport, since the high-energy phonons' excitation rate is faster than their thermalization rate, resulting in a hot phonon generation process [13]. Under that circumstances, one can phenomenologically relax the phonon occupation number in the range of 2–5 [13].

The TDSE is solved by dividing the total evolution time ($t = n\Delta T$) in small time steps ΔT, during which the Hamiltonian energetics is kept constant. This can be expressed as

$$\begin{aligned} |\Psi(t)\rangle &= \exp\left(-\mathrm{i}\frac{\hat{\mathcal{H}}t}{\hbar}\right)|\Psi(0)\rangle, \\ &= \prod_{\alpha=1,n} \mathrm{e}^{-\mathrm{i}H_\alpha \Delta T}|\Psi(0)\rangle \end{aligned} \tag{6}$$

where the whole $\gamma_{ij}(\alpha)$ coupling factors as well as onsite energies (defining H_α) will be modified according to the dynamical motion of atomic coordinates, given by equations (2) and (4). The starting wavepacket is a normalized random phase state that allows efficient treatment of transport in the coherent regime [36]. The γ_{ij} terms are modulated by the phonon modes, encoding the information on phonon frequency, polarization vector and amplitude. The chosen time step is about one tenth of the oscillation period of the considered phonon mode (given in units of $\hbar/\gamma_0$, so $\Delta T = 1$ corresponds to 0.227 fs). We have considered the effect of low-energy modes (acoustic TW mode) with time period of the order of 100 fs, and LO mode for which the period is 20 fs. The chosen time step was $\Delta T = 7(\hbar/\gamma_0) \simeq 1.6$ fs, and the total evolution time $t = 35\,000\hbar/\gamma_0 \sim 10$ ps, so the maximum propagation length for ballistic transport is of the order of 5 μm. Our chosen (10, 10) nanotube has about 20 000 unit cells (total length of $\sim$5 μm), with periodic boundary conditions, a fact that allows us to reduce the boundary effects, as explained elsewhere [36].

3. Low-energy phonons and weak localization phenomenology

The theory of localization in disordered mesoscopic systems is a long-standing issue, based on the quantum interference effects (QIE) on charge transport [20, 21]. These QIE between clockwise and counterclockwise backscattering paths develop in the so-called coherent regime, and yield an increase of the return probability to the origin for propagating wavepackets. The contribution of QIE is usually reduced by several inelastic scattering sources that produce decoherence of the wavepacket phase. At low temperature the main decoherence mechanisms are e–ph and electron–electron couplings. Within the framework of weak localization theory, it has been possible to derive perturbatively the relation between the measured conductance $G(E)$, its quantum correction $\delta G_{\mathrm{WL}}(E)$ and the coherence length L_ϕ that fixes the scale beyond which QIE are destroyed. The estimation of the coherence lengths is a central issue in mesoscopic physics, and weak localization provides an elegant framework to extract the behaviour of L_ϕ, that mainly depends on the dimensionality of charge transport [41, 34].

Stojetz and co-workers [42] have recently succeeded in measuring the energy dependence of the coherence length scale, by using an efficient back-gate electrode able to move the Fermi level position and explore the physics through different subbands. The magnetoresistance data

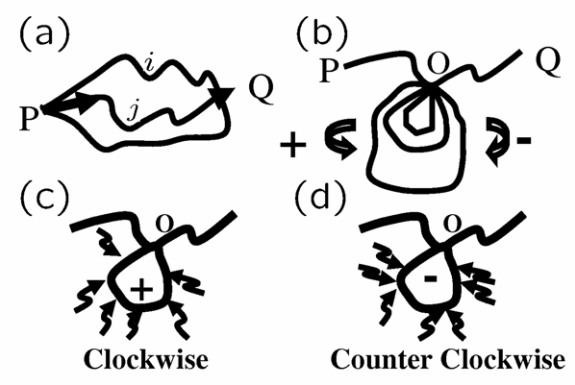

Figure 2. (a) Representation of electronic propagating paths between two points P and Q (a); several paths enclosing a loop returning back to some origin (b), with clockwise (−) and counterclockwise (+) parts; mechanism of decoherence on those paths (arrow indicate inelastic scattering events occurring at different points for (+) and (−) paths.

were well fitted by the conventional theory as [21]

$$\delta G_{\mathrm{WL}} = -A\frac{e^2}{\pi\hbar L}\left(\frac{1}{L_\phi^2}+\frac{W^2e^2B^2}{3\hbar^2}\right)^{-1/2}, \tag{7}$$

with L the tube length, W the diameter and A a normalization factor. From this expression, the coherence length can be quantitatively extracted. Therefore, by using $L_\phi(T) = (GDL\hbar^2/2e^2k_{\mathrm{B}})^{1/3}T^{-1/3}$, the diffusivity was deduced $D = 100\ \mathrm{cm}^2\ \mathrm{s}^{-1}$ (at zero gate voltage) as well as the corresponding elastic mean free path $\ell_{\mathrm{e}} = 2D/v_{\mathrm{F}} \sim 20$ nm. By reproducing this calculation at several values of the gate voltage, a corresponding energy-dependent pattern was revealed. The spectacular observation was the systematic decrease of L_ϕ (as well as ℓ_{e}) near the onsets of each new subband (van Hove singularity positions). Although the energy dependence of ℓ_{e} as was revealed numerically [36], the energy dependence of L_ϕ was to date unexplored.

Finally, by studying the temperature dependence of L_ϕ, the decoherence mechanism was attributed to electron–electron scattering, in agreement with conventional theory. Electron–electron and e–ph scattering are two different sources of quantum dephasing, but within weak localization theory the resulting decoherence phenomenon is of similar nature, and for instance the derivation of the temperature-dependent coherence time follows some general formal treatment [43, 34, 44].

Here, based on all those observations, we investigate the energy dependence of the coherence length scales in carbon nanotubes in the situation where e–ph interaction becomes the dominant source of decoherence.

The physical origin of the coherence length can be simply understood as follows. First, weak localization corrections are evaluated when computing the conductance for wavepacket propagation between two real space positions, let us say from P to Q: $G = \frac{2e^2}{h}\mathcal{P}_{\mathrm{P}\to\mathrm{Q}}$, which can be further expanded as $\mathcal{P}_{\mathrm{P}\to\mathrm{Q}} = \sum_i |\mathcal{A}_i|^2 + \sum_{i\neq j}\mathcal{A}_i\mathcal{A}_j\mathrm{e}^{\mathrm{i}(\alpha_i-\alpha_j)}$, where the summation over probability amplitudes (denote $\mathcal{A}_i$) includes all possible electronic pathways i (see figure 2 for illustration). Here one separates the total probability between the classical and interference parts. Then averaging over (elastic) disorder configurations reduces the contribution of interference terms to a single class, namely the paths that include a finite loop which return

to some initial point, let us say O, that can be further expressed analytically as

$$\mathcal{P}_{O\to O} = |\mathcal{A}_+ e^{i\alpha_+} + \mathcal{A}_- e^{+i\alpha_-}|^2 = 4|\mathcal{A}_0|^2, \tag{8}$$

since clockwise and counterclockwise probability amplitudes have the same phase factor in the case of time reversal invariance [34]. Weak localization thus results from the enhancement (doubling) of the return probability to the origin, with a consequent increase of quantum resistance.

To understand decoherence, one must realize that when inelastic mechanisms come into play on top of coherent transport, then clockwise and counterclockwise pathways accumulate a different superimposed random phase factor $e^{i\alpha_+} = \langle e^{+i\phi}\rangle = \int d\phi\, P(\phi) e^{i\phi}$ and $e^{i\alpha_-} = \langle e^{-i\varphi}\rangle = \int d\varphi\, P(\varphi) e^{-i\varphi}$, respectively. These expressions are derived by considering that the coherent propagating wavepackets are coupled to some external fluctuating potential, such as a thermal bath or fluctuating electromagnetic field that respectively encode the e–ph and electron–electron interaction processes [44]. $P(\phi)$ denotes the probability distribution function for the phase φ, that results from the combination of inelastic and elastic scattering processes, both having a probabilistic nature along the electronic paths (figures 2(c) and (d)). Besides, if $\mathbf{u}(\mathbf{r}, t)$ defines the phonon displacement field, these phase factors are physically related to the Lagrangian of the system, through its action along the electronic pathways, giving [44]

$$\phi, \varphi = \frac{m_c}{\hbar} \int dt\, \mathbf{v} \cdot (\mathbf{v} \cdot \nabla)\mathbf{u}(\mathbf{r}, t) - \frac{1}{d}\mathbf{v}^2 \nabla \cdot \mathbf{u}(\mathbf{r}, \mathbf{t}), \tag{9}$$

with m_c the atomic carbon mass, d the space dimensionality, and $\mathbf{r}$, $\mathbf{v}$ describing the position and related velocity of the electronic pathways [44], while the summation is performed for an elapsed time required to close the relevant loop.

The coherence time τ_ϕ is the time beyond which a full uncertainty of the phase difference is achieved between clockwise and counterclockwise paths (that is when the width of the distribution $P(\varphi)$ becomes of the order of $\sim 2\pi$). Accordingly, the coherence length $L_\phi(E)$ is the length associated with the loop that is closed after an elapsed time $t = \tau_\phi$. Finally, within this phenomenology, the quantum correction of conductance is given by the relevant integrated return probability to the origin [34]:

$$\delta G_{WL} \sim \frac{2e^2 D}{h} \int_0^\infty dt\, \mathcal{P}_{O\to O}(t)(e^{-t/\tau_\phi} - e^{-t/\tau_e}), \tag{10}$$

thus the quantitative measure of conductance correction is driven by the independent calculation of the return probability to the origin in the coherent regime on one side, and estimation of the relevant coherence time on the other side. In the following, our developed computational approach will allow us to evaluate the scaling properties of the quantum correction in the coherent regime, whereas the coherence time will be given by the considered total elapsed time, at which the TDSE will be computed. By doing so, the energy dependence of the weak localization pattern should be correctly reproduced without however providing quantitative information about the exact value of the coherence length scales, or their temperature dependences. This point should be considered on the basis of a microscopical modelling of e–ph interaction and rigorous quantum mechanical treatment of inelastic transport.

One must notice that weak localization has not been reported in single-walled nanotubes, but only in multiwalled carbon nanotubes, in which the Fermi level position is likely to lie within higher massive energy subbands. This is not surprising since transport physics in single-walled nanotubes is dominated by the massless subband (close to the charge neutrality point), and due to the pseudospin symmetry, the backscattering is anomalously small [4], as well as its further weak localization correction [35]. This observation has also been reported in

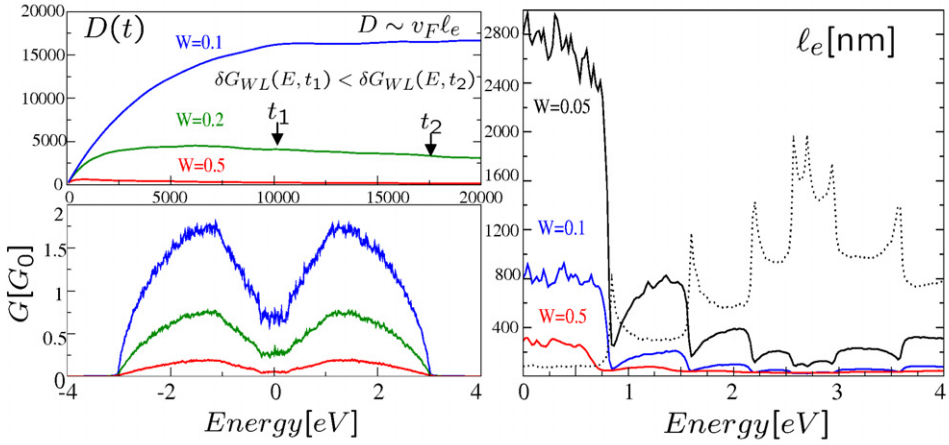

Figure 3. Left panel: (top) time dependence of the diffusion coefficient ($D(t)$) for several values of Anderson disorder W. Time is in $\hbar/\gamma_0$ units, whereas D is in $\text{Å}^2\gamma_0/\hbar$ units; (bottom) energy dependence of the Kubo conductance for the corresponding disorder potentials. Right panel: energy dependence of the ℓ_e, with superimposed density of states (dashed line) to pinpoint the onsets of new subbands.

experiments on multiwalled nanotubes by exploring weak localization through massless and massive subbands [42].

In our formalism, the resolution of the TDSE is made by expanding the evolution operator $e^{-i\hat{\mathcal{H}}t}$ as a product of short-time evolution steps $e^{-i\hat{\mathcal{H}}\Delta T}$, for a total evolution time $t = n\Delta T$. Typically ΔT is one tenth of the oscillation period of the considered phonon mode. During each elapsed time ΔT, the Hamiltonian energetics is fixed by the static part of the *Anderson potential*, whereas the time-dependent part, due to long-range vibrational modes, varies in conjunction with the associated overlap integral modulations. A similar treatment of dephasing has been implemented either by defining an artificial oscillating behaviour of off-diagonal electronic couplings [38], or through an onsite time-dependent perturbation [45]. In [38], scaling properties of the quantum conductance were analysed in the weak localization regime, whereas the metal–insulator transition was investigated in [45].

The Kubo conductance is related to the diffusion coefficient $\text{Tr}[\delta(E-\hat{\mathcal{H}})(\hat{\mathcal{X}}(t)-\hat{\mathcal{X}}(0))^2]/\text{Tr}[\delta(E-\hat{\mathcal{H}})]$, where $\delta(E-\hat{\mathcal{H}})$ is the spectral measure operator, whose trace gives the total density of states, while $\hat{\mathcal{X}}(t)$ is the position operator in the Heisenberg representation. From the time dependence of $L^2(E,t) = \langle\Psi(0)|(\hat{\mathcal{X}}(t)-\hat{\mathcal{X}}(0))^2|\Psi(0)\rangle$, one derives the scaling properties of the conductance [36], together with the conduction regime. The presence of lattice defects produces elastic scattering of the π-electrons, and leads to a transition of the quantum spreading from a ballistic-like to a diffusive regime, at which the diffusion coefficient will saturate. This allows us to estimate the intrinsic elastic mean free path from $L^2(E,t)/t \to \ell_e v(E)$ for a given disorder strength.

In the right panel of figure 3, ℓ_e is shown for three amplitudes of the elastic disorder potential $W = \{0.07, 0.1, 0.5\}\gamma_0/\hbar$. Close to the CNP, $\ell_e(E=0)$ can be computed analytically within the FGR. Indeed, $\ell_e = v_F\tau_e$, with $v_F = 3a_{cc}\gamma_0/2\hbar$ the Fermi velocity ($a_{cc} = 1.44$ Å), whereas τ_e is the elastic scattering time. For the Anderson disorder potential, an analytical derivation provides [3, 36]

$$\ell_e = \frac{18a_{cc}\gamma_0^2}{W^2}\sqrt{n^2+m^2+nm}. \tag{11}$$

The obtained values for ℓ_e at the CNP are given by $\ell_e(E = 0, W = 0.05\gamma_0) = 2800$ nm, $\ell_e(E = 0, W = 0.1\gamma_0) = 800$ nm and $\ell_e(E = 0, W = 0.5\gamma_0) = 37$ nm. Note that in figure 3, $\ell_e(W = 0.5\gamma_0) \to 8 \times \ell_e(E = 0, W = 0.5\gamma_0)$, for the sake of clarity. One thus finds that $\ell_e(W = 0.05)/\ell_e(W = 0.1) \simeq 3.5$, whereas $\ell_e(W = 0.05)/\ell_e(W = 0.5) \simeq 80$, in good agreement with the $1/W^2$ scaling given by equation (11). At higher energies, ℓ_e decreases significantly with some modulations at the onsets of new subbands.

By defining $\tau(L)$ the time at which $L^2(t) = L^2$, the conductance at such scale is defined by $G \simeq e^2 n(E) L(\tau(L))/\tau(L)$ [36]. In figure 3 (left panel), the quantum conductance is shown for the same parameters for random potential. The superimposition of the additional time-dependent part encoding the TW mode (not shown here) does not bring significant changes. At $W = 0.0$ the effect of phonon vibrations is negligible in most of the spectrum, except at some particular energies ± 0.2 eV, that correspond to a particular phonon-induced symmetry-breaking effect [15]. For disorder $W = \{0.07, 0.1\}\gamma_0/\hbar$, the conductance takes values much smaller than in the ballistic case ($W = 0$ and $G(E) = N_\perp G_0$, with $N_\perp$ the number of available channels, $G_0 = 2e^2/h$), and the superimposed effect of phonons remains weak.

To extract the information about the energy dependence of the coherence length scales, we proceed as follows. In the weak localization regime, the quantum correction of the Drude conductance is computed by solving the so-called Cooperon equation [34]. Assuming a quasi-1D geometry of the system, it has been shown that decoherence either due to e–ph or electron–electron scattering is described by the same approach [43], and that the conductance reads

$$G_{\text{Kubo}}(E) = \frac{2e^2}{h}\left(N_\perp(E)\frac{\ell_e(E)}{L(E,t)} - \delta G_{\text{WL}}(E)\right), \tag{12}$$

where $L(E, t)$ is the length scale that is energy dependent due to the velocity $v(E)$, and scales as $L(E, t) = \sqrt{v(E)\ell_e t}$ in the diffusive regime, whereas the term $\delta G_{\text{WL}}(E)$ gives the contribution of QIE beyond the scale of ℓ_e. Within the weak localization theory, and for quasi-1D systems, this contribution is shown to be related to the coherence length $L_\phi(E)$ as $\delta G_{\text{WL}}(E) = L_\phi(E)/L(E, t)$ whereas

$$\tau_\phi(E) = L_\phi^2(E)/v(E)\ell_e. \tag{13}$$

Therefore, by exploring the scaling behaviour of $\delta G_{\text{WL}}(E)$, one can access relevant physical information about the fluctuations of the coherence length scales in the weak localization regime.

Figure 4 (left panel) shows the conductance computed at two different evolution times, $t = 3500\hbar/\gamma_0$ and $t = 35\,000\hbar/\gamma_0 \simeq 8$ ps (dashed curves). One clearly sees a downscaling of the conductance with time, that comes from the classical linear downsizing in the diffusive regime $\ell_e(E)/L(E, t)$, together with the increasing QIE contribution of $\delta G_{\text{WL}}(E, t)$ with time (or equivalently length) scale. In the same figure, we also report the classical term $G_{\text{class}}(E) = N_\perp(E) G_0 \ell_e(E)/L(E, t)$ (bold curve), along with the quantum interference term $\delta G_{\text{WL}}(E, t) = G_{\text{Kubo}}(E, t) - G_{\text{class}}(E)$ (dotted curve), at $t = 35\,000\hbar/\gamma_0$. These results are obtained for $W = 0.07\gamma_0$ and no phonon dephasing, and adding the time dependence modulations of the integral overlap associated to the TW mode does not bring any appreciable changes [37].

Figure 4 (right panel) gives $L_\phi(E)$ (main frame) and $\tau_\phi(E)$ (inset) deduced from equation (12) for $W = \{0.1\gamma_0, 0.2\gamma_0, 0.5\gamma_0\}$ (bold, dotted and dashed curves respectively). The values range within (10 nm, 1000 nm) in the considered energy window. One notes that for energies $\leqslant 0.9$ eV and within the considered evolution time, the quantum correction $\delta G(E) \simeq 0$, so no meaningful information about the coherence length can be deduced since the transport remains quasi-ballistic. In contrast, the coherence time shows reversed behaviour, owing to the strong decrease of ℓ_e.

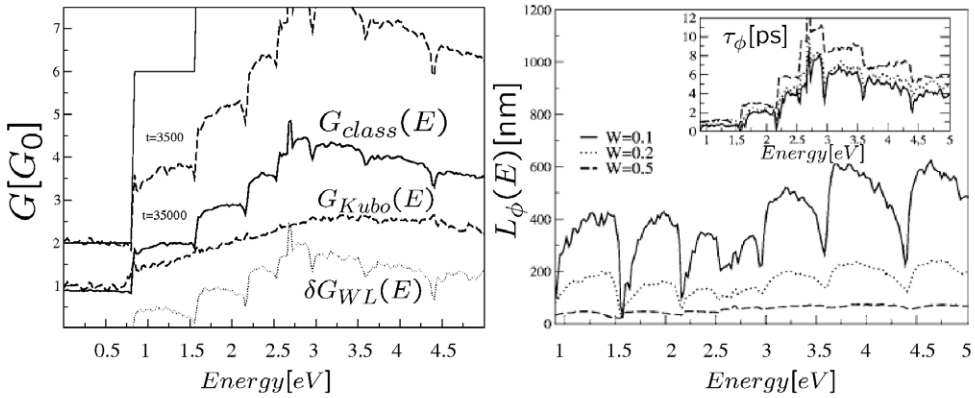

Figure 4. Left panel: conductance for the disordered (10, 10) tube with $W = 0.07\gamma_0$, taken at evolution times $t = 3500\hbar/\gamma_0$ and $t = 35\,000\hbar/\gamma_0$ (dashed curves). The bold curve gives the classical part $G_{\rm class}(E) = G_0 N_\perp \ell_{\rm e}(E)/L(E,t)$, whereas the dotted curve gives the quantum correction $\delta G_{\rm WL}(E)$ ($t = 35\,000\hbar/\gamma_0$). Right panel: coherence lengths deduced from $\delta G_{\rm WL}(E) = L_\phi(E)/L(E)$ computed at $t = 35\,000\hbar/\gamma_0$, and for several values of disorder potential. Inset: corresponding $\tau_\phi(E)$ for the same parameters. In addition to the random short-range disorder, a TW mode modulation is introduced.

In the experimental situation [42], the fluctuations of $L_\phi(E)$ due to electron–electron scattering were found to scan the range (10 nm, 60 nm), with systematic decrease near the onsets of new subbands. The values given here (for the chosen evolution time) are thus physically reasonable, since e–ph scattering is expected to lead to weaker decoherence effect [43]. In the following section we show how these e–ph inelastic scattering rates can be calculated by using the Fermi golden rule.

4. Relaxation time and mean free path in armchair tubes by the Fermi golden rule

Hereafter, we compute the inelastic electronic transport length scales (mean free paths) associated to a selected vibrational mode coupling. The scattering rate is evaluated from the Fermi golden rule [25, 47], assuming that the e–ph coupling that induces the electronic transition remains perturbative in the sense that it can be described by first-order perturbation theory, with equilibrium distributions for both electrons and phonons. Several computational approaches can be used, from first-principles calculations to extended tight-binding methods or hybrid approaches. Here the latter one is followed and the results presented are obtained using an extended tight-binding model based on density functional calculations.

The starting Hamiltonian assumes independent electrons moving in the crystalline potential $H = -(\hbar^2/2m)\nabla^2 + V$, where the first and second terms are, respectively, the kinetic and potential energies, with $V = \sum_{\mathbf{R}_i} v(\mathbf{r} - \mathbf{R}_i)$ and v is the Kohn–Sham potential of a neutral pseudoatom [39]. The periodic displacements of atoms around equilibrium positions $\mathbf{R}_i^0$ described by the relevant vibronic modes give rise to the e–ph coupling

$$\begin{aligned}\delta V &= \sum_{\mathbf{R}_i^0} v[\mathbf{r} - \mathbf{R}_i^0 - \mathbf{S}(\mathbf{R}_i^0)] - v(\mathbf{r} - \mathbf{R}_i^0) \\ &\approx -\sum_{\mathbf{R}_i^0} \nabla v(\mathbf{r} - \mathbf{R}_i^0) \cdot \mathbf{S}(\mathbf{R}_i^0), \end{aligned} \tag{14}$$

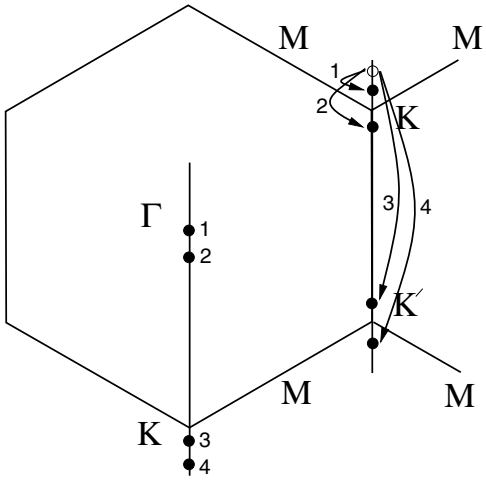

Figure 5. The e–ph scattering processes near the Fermi level (the K and K′ points) of an armchair tube. The processes 1 and 2 are the intravalley forward and backward scattering and the corresponding phonons are around the Γ point. Processes 3 and 4 are the intervalley forward and backward scattering respectively, and the corresponding phonons are around the K point.

where $\mathbf{S}(\mathbf{R}_i^0)$ is the site position deviation from the equilibrium site $\mathbf{R}_i^0$ caused by a vibration. The vibration $\mathbf{S}(\mathbf{R}_i^0)$ for the phonon mode $(\nu, \mathbf{q})$ is related to the phonon amplitude, polarization vector and energy. The inelastic scattering rate between an electronic state $|\Psi_{\alpha,\mathbf{k}}\rangle$ from band α, with momentum $\mathbf{k}$ and energy $\varepsilon_{\alpha,\mathbf{k}}$, and another $|\Psi_{\alpha',\mathbf{k}'}\rangle$ with different energy, due to a phonon of momentum $\mathbf{q}$ in branch ν and energy $\hbar\omega_\nu(\mathbf{q})$ can be derived by the first-order perturbation theory (FGR) as [13, 25]:

$$1/\tau = \frac{2\pi}{\hbar} n_\nu(\mathbf{q})|M|^2\rho, \tag{15}$$

with ρ the density of states for the final states, M the e–ph matrix element, and n_ν the phonon number, as defined earlier.

The e–ph matrix element between states $|\Psi_{\alpha,\mathbf{k}}\rangle$ and $|\Psi_{\alpha',\mathbf{k}'}\rangle$ is calculated by the deformation potential [46],

$$M_{(\mathbf{k}+\mathbf{q})\alpha',\mathbf{k}\alpha} = \langle\Psi_{\alpha',\mathbf{k}+\mathbf{q}}|\delta V|\Psi_{\alpha,\mathbf{k}}\rangle. \tag{16}$$

It is convenient to introduce an unnormalized e–ph matrix element D by [46]

$$M = -\sqrt{n_\nu(\mathbf{q})\hbar/(N_\mathrm{u} m_\mathrm{c}\omega_\nu(\mathbf{q}))}\,D, \tag{17}$$

with N_u the number of graphene unit cells in the SWNT. The density of states ρ is

$$\rho = N_\mathrm{u} S/\pi d_t \hbar v_\mathrm{F}, \tag{18}$$

with S the area of a 2D graphene unit cell [25, 47] and v_F the electron velocity near the Fermi level.

For armchair SWNTs, the cutting line [49] for metallic bands passes through the edge KK′ of the 2D Brillouin zone (BZ) shown in figure 5. Near the Fermi level there are four kinds of e–ph scattering processes. The phonon modes for intravalley forward and backward scattering (processes 1 and 2 in figure 5) are those around the Γ point modes. The phonon modes for intervalley forward and backward scattering (processes 3 and 4 in figure 5 are those around the K point modes. Therefore, for e–ph scattering near the Fermi level, we have six Γ-point modes, i.e., longitudinal acoustic (LA), TW, radial breathing (RBM), out-of-plane transverse

Table 1. The e–ph coupling strength $|D|$, relaxation time τ, and mean free path ℓ for each mode near the Fermi level of a (10, 10) tube. The wavevector q used to express $|D|$ for the TW mode is in units of Å^{-1}.

		Forward			Backward		
Mode	Freq. (cm^{-1})	$\lvert D\rvert$ (eV Å^{-1})	τ (ps)	ℓ (nm)	$\lvert D\rvert$ (eV Å^{-1})	τ (ps)	ℓ (nm)
LA	0	0	0		0	0	
TW	0	0	0		$2.462q$	2.14	1812.2
RBM	187.10	1.53	0.56	469.9	0	0	
oTO	889.85	0	0		9.94	1.25	8354.1
TO	1591.51	7.17	0.56	470.1	0	0	
LO	1595.51	0	0		6.66	0.65	546.8
E_2' (1)	527.69	1.91	1.57	1 320.0	0	0	
E_2' (2)	545.47	0	0		0.95	8.72	7326.6
A_2'	988.82	0.48	39.6	33 267.3	0	0	
E_1' (1)	1231.76	11.22	0.18	154.6	0	0	
E_1' (2)	1249.52	0	0		10.82	0.20	165.6
A_1'	1368.88	0	0		9.94	0.27	228.2

optical (oTO), TO, and LO, and six K-point modes, i.e., two E_2' modes, a A_2' mode, two E_1' modes, and a A_1' mode.

In table 1, we list the e–ph coupling strength ($|D|$), relaxation time (τ) and mean free path (ℓ) of a (10, 10) tube for each mode for electrons with an initial state energy 0.25 eV above the Fermi level [46]. The phonon frequencies for the modes near the Γ and K points are also listed. For a given energy, there are two initial states around a K point with one on the line ΓK and the other on the line KM. In table 1, $|D|$ is the averaged value for the two points on the ΓK and KM lines, i.e., $|D| = (|D|_{\Gamma\text{K}} + |D|_{\text{KM}})/2$. The matrix element $|D|$ has similar values for emission and absorption processes. In table 1 we only show $|D|$ for emission processes.

Table 1 indicates that for acoustic phonon modes, the e–ph coupling for back scattering mainly comes from the TW mode, and the resulting mean free path can be longer than 1 μm, which agrees with the transport measurements on SWNTs with low bias voltage [50, 10]. For high-energy phonon modes, the e–ph coupling of back scattering is dominated by the LO, A_1' and one of the E_1' modes. The resulting mean free path for a (10, 10) tube is about 76.6 nm, which agrees with that reported by other calculations [5, 10, 15]. In our calculations, a thermal equilibrium at a temperature $T = 300$ K is assumed. For low-energy phonons, ℓ is inversely proportional to T, while for high-energy phonons, ℓ is independent of T. The above conclusion is valid only under thermal equilibrium conditions. In the case of thermal unequilibrium, hot phonons will help to reduce ℓ.

For metallic tubes in the low-bias and high-bias ranges, we get two simple expressions for the scattering length, respectively, $\ell_{\text{TW}} = 400.46 \times 10^3 d_t/T$ and $\ell_{\text{op}} = 56.4 d_t$, where ℓ_{TW} is in units of nm.

In this section we have presented a scheme to calculate the e–ph scattering rates based on the FGR. However, as we will see in the next section, experimental estimations [9, 5, 10] of these rates gives e–ph scattering lengths of the order of 10–15 nm. This order of magnitude difference motivated the proposal of a hot phonon scenario in [13].

5. Current-carrying capacity in metallic carbon nanotubes and current saturation

The strong current-carrying capacity of carbon nanotubes opens novel possibilities to improve the performances of nanoscale devices either in the field of interconnects or field effect

transistors. The study and understanding of current–voltage characteristics of both metallic and semiconducting nanotubes is thus a crucial point to fix the limits for further technological applications.

Yao and co-workers were the first to explore the $I(V)$ characteristics of metallic tubes in the high-voltage regime [9]. Their study of small-diameter metallic tubes with low contact resistance to the voltage probes shows a linear regime followed by a saturation regime for voltage of the order of 1 V, weakly temperature dependent. The overall $I(V)$ characteristic is described by a law

$$I = \frac{V}{R_0 + V/I_0}, \tag{19}$$

with R_0 and I_0 two constants giving respectively a voltage-independent intrinsic resistance and a current saturation value (weakly dependent on the diameter of the nanotube), and found to be of the order of 20–30 μA. The interpretation assumes that the saturation comes from the strong inelastic backscattering of electrons coupled to optic (or zone boundary) vibrational modes. In this scenario, the inelastic mean free path is the length the electrons need to traverse to accumulate an additional energy of $\hbar\Omega_{\rm ph}$, which is the energy of the relevant phonon mode that at this point is *assumed to be instantaneously activated and that will backscatter electrons with unit probability*. Assuming a linear potential drop between voltage probes separated by L, i.e. $V(l) = V_{\rm bias}(1 - l/L)$, l being the distance from the source, then the energy gain reads $e\int_0^{\ell_{\rm ie}} \partial V/\partial l \, {\rm d}l = \hbar\Omega_{\rm ph}$, from which one straightforwardly deduces that $\ell_{\rm ie} = (\hbar\Omega_{\rm ph}L)/eV_{\rm bias}$. Besides, assuming that the length-dependent resistance can be split into two contributions, by virtue of the Mathiessen rule, one writes

$$R(L) = \frac{h}{4e^2}\frac{L}{\ell_{\rm e}} + \frac{h}{4e^2}\frac{L}{\ell_{\rm ie}} = R_0 + \frac{h}{4e^2}\frac{eV_{\rm bias}}{\hbar\Omega_{\rm ph}} = R_0 + \frac{V_{\rm bias}}{I_0}, \tag{20}$$

with $R_0 = h/4e^2 L_{\rm tube}/\ell_{\rm e}$ the intrinsic resistance and $\ell_{\rm e}$ the elastic mean free path, whereas $I_0 = (4e/h)\hbar\Omega_{\rm ph}$, which is indeed equal to 20–30 μA depending on the chosen phonon energy. One notices that, whereas $\ell_{\rm e}$ is an intrinsic measure of the elastic disorder strength (defect density, etc) which is a bias- and temperature-independent quantity, $\ell_{\rm ie}$ is voltage dependent in this model, but at a fixed voltage it should remain inversely proportional to the nanotube length. Intriguingly, however, by using a semiclassical Boltzmann approach, a fitting of the experimental data is achieved taking a fixed $\ell_{\rm ie}$ (for a fixed tube length) independent of the voltage bias [9].

The observation of a length-dependent scaling of the resistance has been reported in several works [10, 51, 5]. Lower resistances are measured for shorter tubes, and current saturation was shown to be reduced when decreasing $L_{\rm tube}$ from 700 to 50 nm, at which no saturation was observed for voltage bias up to 1.5 V. Again, analysis within the Fermi golden rule and Boltzmann approach allows one to deduce some typical values for the inelastic scattering lengths that can be as short as 10 nm [5]. The discrepancy or strong fluctuations between estimates obtained by fitting procedures and the computed $\ell_{\rm ie}$ (with FGR) either as reported in the prior section or in other *ab initio* works [18, 19] raises some fundamental questions about the applicability of the Fermi golden rule, Mathiessen rule and semi-classical transport theory to tackle inelastic quantum transport in metallic carbon nanotubes, or within the context of carbon nanotube-based field effect transistors [6]. As discussed below, our developed methodologies suggest some failure of these semiclassical approaches in analysing quantum transport in nanotubes in the presence of high-energy vibrational modes.

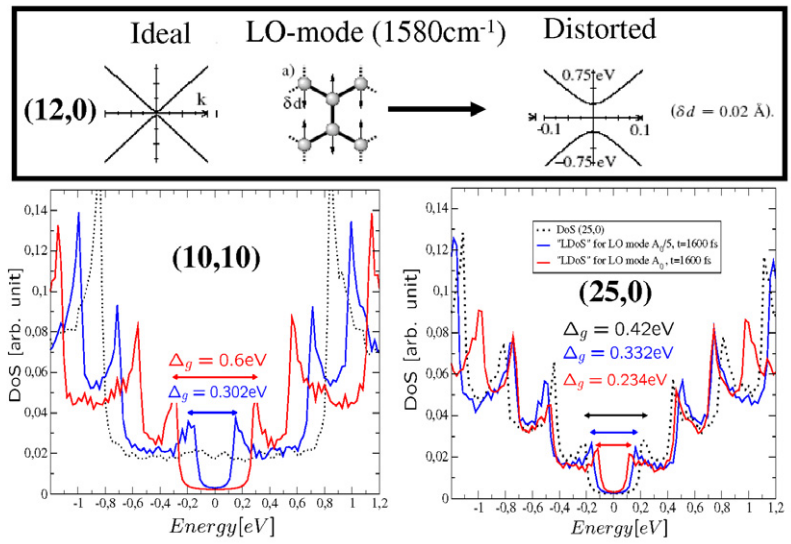

Figure 6. Top panel: *ab initio* calculation of dynamical effect of the LO mode on the band structure (adapted from [48]). Bottom panel: density of states for a metallic (10, 10) tube (left) and a semiconducting (25, 0) tube (right) with e–ph coupling. The effective phonon amplitude for the (10, 10) is A_0 ($\Delta g = 0.302$ eV), $2A_0$ ($\Delta g = 0.6$ eV) for the (10, 10) while for the (25, 0), A_0 ($\Delta g = 0.332$ eV) at $t = 1600$ fs. Dashed lines give the density of states of nanotubes without phonon modulation.

6. Effect of high-energy phonons within the time-dependent description

The effect of high-energy optic modes on the band structure was first studied by Dubay and co-workers [48]. In their work, a comparison between equilibrium band structure and the electronic spectrum of a distorted nanotube, encoding the atomic displacements of high-energy modes, demonstrates the occurrence of shifts of the electronic bands, that scale linearly with the distortion amplitude (see also [26] for armchair tubes).

In [48], the band structure changes of a metallic zig-zag nanotube (the case of (12, 0)) due to e–ph coupling was investigated. In the vanishing e–ph coupling situation, the electronic structure shows a very small bandgap due to curvature effects. Then by considering the LO (1591 cm^{-1}), they introduce the relative displacement δd of the π orbital position with respect to the equilibrium position (see figure 6 top panel). The band structures for several values of such scaling parameter are then computed with an *ab initio* (density functional theory) method. As a result, a bandgap oscillation is found, whose value is reported to follow $\Delta_g = 26$ eV $\text{Å}^{-1}|\delta d|$, whereas no detailed information about the rest of the spectrum is given. By using the computational approach introduced in section 2, we investigate the time dependence of the density of states. In figure 6, one shows the density of states for the (10, 10) tube (bottom left) evaluated at time $t \sim 1600$ fs $\sim 80T_{\text{LO}}$. We show the result for a doubling in amplitude of the phonon mode. Similarly to [48], the doubling of the displacement results in a doubling of the energy gap, which equals $\Delta_g = 0.302$ eV for A_0. Following the time dependence of the density of states, we recover a complex modification of the full energy spectrum with shifts of the van Hove singularities that cannot however be easily understood analytically. The case with a semiconducting (25, 0) tube is also shown (bottom right) for three values of the phonon amplitudes.

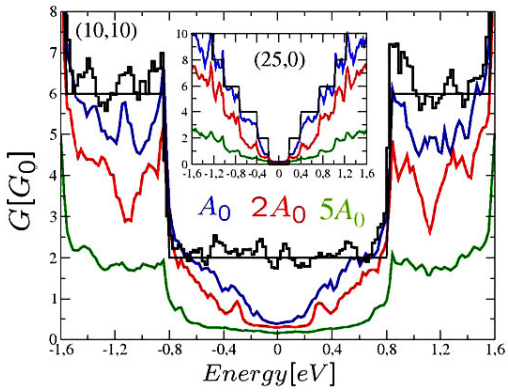

Figure 7. Conductance for a metallic (10, 10) tube (main frame) and a semiconducting (25, 0) tube (inset) with e–ph coupling (LO mode). The effective phonon amplitude is from bottom to top curve: $5A_0$, $2A_0$, A_0. The solid lines give the exact number of quantum channels $N_\perp$. For the (10, 10) case, the $A_0 = 0$ numerical calculation and the exact number of quantum channels are also shown.

Such effects of the time-dependent modulations of the band structure are obviously at the origin of the subsequent alteration of the conductance scaling properties, if one considers its remaining coherent part. As discussed later on, this point should be considered with care at the time of using semiclassical transport theories and the FGR to describe relevant transport length scales of current–voltage characteristics of CNT-based devices.

As shown in figure 7, the modifications of the electronic conductance $G(E)$ due to coupling to optic LO modes are strong in the central region around the CNP, as well as for higher energies. Besides, the scaling properties of conductance patterns are found to fluctuate owing to time-dependent band structure changes. Besides, by considering the hot phonon occupation scenario and the enhanced e–ph coupling by the A_1' phonon, we let the amplitude vary within $[A_0, 5A_0]$. The conductance as a function of Fermi energy and amplitude of the e–ph coupling are shown for a typical (10, 10) metallic nanotube (figure 7—main frame) and a (25, 0) semiconducting nanotube (figure 7—inset). The increase of phonon amplitude progressively degrades the conductance all over the spectrum, although some fluctuations are seen in the surroundings of the van Hove singularities. Close to the onsets of new subbands (defined by the energies of the van Hove singularities), the conductance remains larger in regard to the rest of the spectrum. This originates from the reduced velocity of charge carriers at those energies, that results in lower propagating length $L(E, t) = v(E)t$ (for the same evolution time t), and weaker contribution of e–ph coupling. Note that different phonon amplitudes also result in some band structure changes, that are reflected in the energies where the conductance of the A_0 case becomes smaller than the $2A_0$ case (only seen for the (10, 10) tube).

Such behaviour found within the Kubo framework, and illustrated in figure 6 seems to indicate that high-energy phonon modes have an impact in the conductance even in the linear response regime. This clearly brings some contradiction in the sense that in this regime (low-bias limit) there is no phase space for inelastic processes, which are forbidden by Pauli blocking. Therefore, how should we interpret these results?

To that end, one should notice the following points: (a) in this time-dependent description, the 'phonon modes' are intrinsically activated since the atoms are forced to vibrate with a well-defined amplitude and phase; (b) the Pauli principle is not properly taken into account in this one-body description. Hence, these results should be interpreted as the conductance in a non-

equilibrium situation in which the phonon modes are activated through a finite bias voltage; however, the approximation of the linear response (Kubo) prevents us from fully addressing the high bias voltage regime.

Another limitation of this approach is that processes of phonon emission and absorption cannot be rigorously distinguished, at least by keeping a real e–ph interaction Hamiltonian. As a consequence, a zero-temperature situation (in which no phonon absorption is allowed) cannot be described within this framework. In the next section, we propose to go beyond the limitations of the Kubo approach, by adopting a many-body treatment of inelastic transport.

7. High-energy phonons and many-body treatment of inelastic transport

The results shown before clearly hint at the importance of two ingredients of the e–ph interaction in electronic transport through CNTs. One is the symmetry of the phonon mode under study, which is given by the phonon polarization vectors. The fact that the phonon frequency is high adds an important dynamical input to the problem. In principle, this should limit the possibility of restricting ourselves to a mean-field description of the e–ph Hamiltonian [52]. The interplay between these two ingredients leads to a wealth of novel coherent phenomena as evidenced by recent experiments [53] and theory [32]. Recently, other subtle coherent phenomena have also been proposed [54].

The time-dependent description used in the previous section incorporates these two ingredients and constitutes a first step along this direction. Formally it can be seen as a semiclassical approximation for the full many-body problem where the phonon operators are replaced by a time-periodic function with well-defined amplitude and phase, thereby giving a one-body time-dependent problem. Several questions naturally arise: What are the limitations of this scheme? What are the ingredients that are missing as compared to a full many-body description? An attempt to answer these questions within a unified framework will be presented below along the lines given in [33].

Our aim is to make evident to the reader the need of using a full many-body description of the e–ph interaction that: (a) accounts for the proper symmetry of the considered phonon modes; (b) allows the study of the nonlinear response regime; (c) allows a non-perturbative description of the e–ph interaction. The importance of (a) and (b) was evidenced in [32], where the interaction with the LO mode in CNTs was shown to lead to phonon-induced energy gaps at high bias. We will comment more on this issue later.

Another important issue concerns the out-of-equilibrium phonon population. If the phonons are not able to equilibrate in a time that is rapid compared to the mean time between successive electrons entering the device, the phonon population, which can be characterized by the probability distribution P_n (n being the number of phonons), is driven out of equilibrium. In this respect, recent studies involving ballistic CNTs [13, 18, 19] and CNTs in the Coulomb blockade regime [55] propose a hot phonon scenario in order to explain the quantitative disagreement between theoretical and experimental estimations of inelastic mean free paths in CNTs.

On the other hand, in [56] Mitra *et al* presented counterintuitive numerical results which show that the phonon probability distributions are farther from equilibrium for weak e–ph couplings than for strong ones. These intriguing results were confirmed by analytical calculations carried out in the small e–ph coupling limit by Koch *et al* [57]. Specifically, they found [57] that the width of the phonon probability distribution diverges as $(\gamma^{\mathrm{e-ph}})^{-\zeta}$ when the e–ph coupling strength $\gamma^{\mathrm{e-ph}}$ decreases. As a consequence, in non-equilibrium conditions, a breakdown of perturbation theory in the e–ph coupling is possible. This opens new exciting issues for future research on non-equilibrium phonons. Besides, this points out the need to go beyond perturbative approaches for the e–ph interaction.

In the following we introduce a suitable Hamiltonian description for the e–ph interaction and outline a many-body scheme that allows the description of quantum inelastic transport as developed in [32].

7.1. Hamiltonian description for the e–ph interaction

In this section we will revisit the Hamiltonian description of the effects of vibrations on the electronic transport. Our aim is to give some unified picture for the time-dependent description given in the previous sections and a full many-body scheme. Our starting point is the modelling of the Hamiltonian for the e–ph system. For simplicity, an infinite CNT is considered and the electrons are allowed to interact with phonons only in the central part of the CNT. The Hamiltonian of the system can be written as a sum of an electronic part, a phonon part and an e–ph interaction term:

$$H = H_{\mathrm{e}} + H_{\mathrm{ph}} + H_{\mathrm{e-ph}}. \tag{21}$$

The electronic part is elaborated through a π-orbital effective model (i.e. a single π orbital per carbon atom) as in section 2:

$$H_{\mathrm{e}} = \sum_i E_i c_i^\dagger c_i - \gamma_0 \sum_{\langle i,j\rangle} [c_i^\dagger c_j + \mathrm{H.c.}], \tag{22}$$

where $c_i^\dagger$ and c_i are the creation and annihilation operators for electrons at site i, γ_0 is the π–π integral overlap; notice that the second summation is restricted to nearest neighbours in the CNT. Let us consider a single phonon mode of energy $\hbar\omega_0$. Then, the phonon term is simply

$$H_{\mathrm{ph}} = \hbar\omega_0 b^\dagger b, \tag{23}$$

where $b^\dagger$ and b are the phonon operators. The last contribution is the e–ph interaction term. Lattice vibrations will produce a time modulation of the bond's length, thereby changing the hopping matrix elements. Our starting point to describe these phenomena is the Su–Schrieffer–Heeger Hamiltonian, where the contribution arising from the phonons is found by assuming a phonon modulation of the hopping matrix elements [52, 58], and keeping only the linear corrections to the atomic displacements from equilibrium. This leads to

$$\gamma_{i,j} = \gamma_0 + \alpha \widehat{\delta}_{i,j} \cdot \delta \vec{Q}_{i,j}, \tag{24}$$

where $\widehat{\delta}_{i,j}$ is a unit vector in the bond direction, whereas $\delta \vec{Q}_{i,j}$ sets the relative displacement of the neighbouring carbon atoms, and α is the e–ph coupling strength defined as the derivative of γ_0 with respect to the bond length displacement. At this point several descriptions are feasible. One possibility is to replace the second term in the previous equation by a time-dependent function with well-defined amplitude and phase [59]. This leads to a Hamiltonian similar to the one introduced in section 2. An alternative is to proceed by performing a further quantization of the atomic displacements. This gives the many-body e–ph interaction term:

$$H_{\mathrm{e-ph}} = \sum_{\langle i,j\rangle_{\mathrm{vib}}} [\gamma_{i,j}^{\mathrm{e-ph}} c_i^\dagger c_j (b^\dagger + b) + \mathrm{h.c.}], \tag{25}$$

where the e–ph interaction is allowed only in a finite section of the CNT of length L, b and $b^\dagger$ are the phonon operators and the e–ph matrix elements $\gamma_{i,j}^{\mathrm{e-ph}}$ are generally given by

$$\gamma_{i,j}^{\mathrm{e-ph}} = \alpha \sqrt{\hbar/(2m\omega_0)}\, \widehat{\delta}_{i,j} \cdot [\mathbf{e}_i^\nu(\mathbf{q}) - \mathbf{e}_j^\nu(\mathbf{q})], \tag{26}$$

where the phonon mode eigenvector $\mathbf{e}_i^\nu(\mathbf{q})$ gives the atomic displacements from the equilibrium positions.

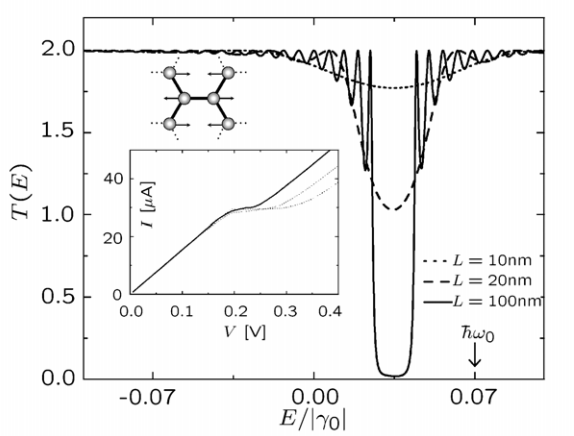

Figure 8. Total transmission probability as a function of the energy of the incident electrons for a zig-zag (24, 0) CNT. The I–V characteristics for different values of the e–ph coupling strength α ($\alpha_0 \simeq 10$ eV, $2\alpha_0$ and $3\alpha_0$) are shown in the inset with solid, dashed and dotted lines respectively. The results correspond to CNTs in the presence of e–ph interaction with an $A_1(L)$ mode inducing displacements along the axis direction (drawings).

In order to solve this many-body Hamiltonian, a strategy is to use the approach introduced in [60, 61] as done in [32] and [33] for transport in CNTs and in [62–66] in other contexts. The main idea behind this approach is to construct an equivalent multichannel one-body problem. This is done by rewriting the Hamiltonian in an appropriate basis for the e–ph Fock space (a single electron plus phonons). The emerging picture is that of a multichannel one-body problem where the asymptotic states in the e–ph Fock space include both the electronic and the new vibrational degrees of freedom; each phonon mode adds an additional dimension to the problem. For more details on this approach we refer the reader to the original papers [60, 61, 65].

The main advantages of this Fock-space approach are three-fold: it is variational in the e–ph interaction, thus allowing a non-perturbative calculation; it allows us to clearly distinguish the contribution from different elastic and inelastic scattering channels; and it allows us to calculate currents both in the linear and nonlinear response regimes.

7.2. Phonon-induced energy and transmission gaps in CNTs

The Fock space approach mentioned before was applied to the case of zig-zag and armchair CNTs in [32, 33] in the presence of e–ph interaction with a single optical phonon mode. The main result is reproduced in figure 8. There, the total transmission is shown as a function of the energy of the incident electrons. Different curves correspond to different tube lengths. The main finding is the appearance of a dip in the transmission at $\hbar\omega_0/2$ above the CNP that progressively deepens to reach a full gap for $L \sim 100$ nm. This gap emerges as the result of the e–ph interaction which removes a degeneracy between many-body states giving a resulting effect which is beyond ordinary perturbation theory. For more details we refer the reader to the original papers [32, 33]. We emphasize that the observed reduction in the transmission probability is complemented by an increase in the inelastic reflection. For sufficiently long tubes and when the phonon mode is activated, this mechanism gives a perfect inelastic backscattering (unit probability) in an energy range around $\hbar\omega_0/2$ above the CNP.

At low bias this effect will be suppressed by Pauli blocking and it develops for bias voltages of the order of $\hbar\omega_0$. The current–voltage characteristics obtained for a simple model for the

potential profile are shown in the inset [32, 33]. Different lines correspond to different values of the e–ph interaction strength. These results show an onset of current saturation at around 30 μA for bias of the order of $\hbar\omega_0$. One notes that this saturation value equals $(4e/h)\hbar\Omega_{\rm ph}$ for perfect contacts.

The current then continues to increase for higher bias, a fact that can be attributed to the lack of other ingredients such as e–ph interaction with other modes, a description of the self-consistent electrostatics and out-of-equilibrium electronic and phonon populations. Nevertheless, this gives a hint to the possible manifestations of this mechanism that to our knowledge has been overlooked in the literature.

8. Conclusions

In summary, we have analysed the effect of electron–phonon interaction with low- and high-energy phonons by using different frameworks. Specifically, we have presented a description based on an effective time-dependent Hamiltonian for the electron–phonon interaction [15] as well as more recent results based on a many body-Hamiltonian [32, 33]. Our results hint at the importance of effects beyond perturbation theory which require a description which takes into account the symmetry as well as the dynamics of the phonon modes. Further work is clearly needed to unveil the role of other phonon modes in transport as well as the possible interplay with electrostatic effects, in the context of understanding carbon nanotube-based field effect transistors [67].

References

[1] Saito R, Dresselhaus G and Dresselhaus M 1998 *Physical Properties of Carbon Nanotubes* (London: Imperial College Press)

[2] Roche S *et al* 2006 *Understanding Carbon Nanotubes From Basics to Applications* (*Springer Lecture Notes in Physics* vol 677) ed A Loiseau, P Launois, P Petit, S Roche and J-P Salvetat (Berlin: Springer)

[3] White C T and Todorov T N 1998 *Nature* **393** 240
McEuen P L *et al* 1999 *Phys. Rev. Lett.* **83** 5098

[4] Ando T, Nakanishi T and Saito R 1998 *J. Phys. Soc. Japan* **67** 2857–62

[5] Javey A *et al* 2004 *Phys. Rev. Lett.* **92** 106804

[6] Appenzeller J, Radosavljevic M, Knoch J and Avouris Ph 2004 *Phys. Rev. Lett.* **92** 048301
Avouris Ph *et al* 2004 *IEDM 2004 Conf. Proc.* p 525
Appenzeller J, Knoch J, Radosavljevic M and Avouris Ph 2004 *Phys. Rev. Lett.* **92** 226802

[7] Javey A, Guo J, Wian Q, Lundstrom M and Dai H 2003 *Nature* **424** 654

[8] Suzuura H and Ando T 2002 *Phys. Rev.* B **65** 235412
Jishi R A, Dresselhaus M S and Dresselhaus G 1993 *Phys. Rev.* B **48** 11385–9
Woods L M and Mahan G D 2000 *Phys. Rev.* B **61** 10651
Pennington G and Goldsman N 2003 *Phys. Rev.* B **68** 045426

[9] Yao Z, Kane C L and Dekker C 2000 *Phys. Rev. Lett.* **84** 2941

[10] Park J-Y, Rosenblatt S, Yaish Y, Sazonova V, Ustunel H, Braig S, Arias T A, Brouwer P and McEuen P L 2004 *Nano Lett.* **4** 517

[11] Pop E, Mann D, Cao J, Wang Q, Goodson K and Dai H 2005 *Phys. Rev. Lett.* **95** 155505

[12] Perebeinos V, Tersoff J and Avouris Ph 2005 *Phys. Rev. Lett.* **94** 086802
Pennington G and Goldsman N 2005 *Phys. Rev.* B **68** 086802

[13] Lazzeri M, Piscanec S, Mauri F, Ferrari A C and Robertson J 2005 *Phys. Rev. Lett.* **95** 236802

[14] Georghe M, Gutierrez R, Ranjan N, Pecchia A, Di Carlo A and Cuniberti G 2005 *Europhys. Lett.* **71** 438

[15] Roche S, Jiang J, Triozon F and Saito R 2005 *Phys. Rev. Lett.* **95** 076803

[16] Svizhenko A and Anantram M P 2005 *Phys. Rev.* B **72** 085430

[17] Kuroda M A, Cangellaris A and Leburton J P 2005 *Phys. Rev. Lett.* **95** 266803

[18] Lazzeri M, Piscanec S, Mauri F, Ferrari A C and Robertson J 2006 *Phys. Rev.* B **73** 155426

[19] Lazzeri M and Mauri F 2006 *Phys. Rev.* B **73** 165419

[20] Thouless D J 1977 *Phys. Rev. Lett.* **39** 1167
Abrahams E *et al* 1979 *Phys. Rev. Lett.* **42** 673

[21] Altshuler B L and Aronov A G 1985 *Electron–Electron Interactions in Disordered Systems* ed A L Efros and M Pollak (Amsterdam: North-Holland) p 1
Altshuler B L, Aronov A G and Spivak B Z 1981 *JETP Lett.* **33** 94
Aronov A and Sharvin Y 1987 *Rev. Mod. Phys.* **59** 755
[22] Collins P G, Hersam M, Arnold M S, Martel R and Avouris Ph 2001 *Phys. Rev. Lett.* **86** 3128
Collins P G, Hersam M, Arnold M S and Avouris Ph 2001 *Science* **292** 706
[23] Bohnen K-P, Heid R, Liu H J and Chan C T 2004 *Phys. Rev. Lett.* **93** 245501
Pennington G and Goldsman N 2003 *Phys. Rev.* B **68** 045426
Woods L M and Mahan G D 2000 *Phys. Rev.* B **61** 10651
Ando T 2005 *J. Phys. Soc. Japan* **74** 777
[24] Kane C L, Mele E J, Fischer J E, Lee R, Petit P, Thess A, Smalley R E, Tans S and Dekker C 1998 *Europhys. Lett.* **41** 683
[25] Jiang J, Saito R, Grüneis A, Chou S G, Samsonidze Ge G, Jorio A, Dresselhaus G and Dresselhaus M S 2005 *Phys. Rev.* B **71** 045417
[26] Hertel T and Moos G 2002 *Phys. Rev. Lett.* **84** 5002
Reich S, Dworzak M, Hoffmann A, Thomsen C and Strano M S 2005 *Phys. Rev.* B **71** 033402
Máchon M, Reich S, Telg H, Maultzsch J, Ordejón P and Thomsen C 2005 *Phys. Rev.* B **71** 035416
[27] Perebeinos V, Tersoff J and Avouris Ph 2005 *Phys. Rev. Lett.* **94** 086802
[28] Perebeinos V, Tersoff J and Avouris Ph 2005 *Phys. Rev. Lett.* **94** 027402
[29] Capaz R B, Spataru C D, Tangney P, Cohen M L and Louie S G 2005 *Phys. Rev. Lett.* **94** 036801
[30] Sédéki A, Caron L G and Bourbonnais C 2002 *Phys. Rev.* B **65** 140515
Blase X, Adessi Ch and Connétable D 2004 *Phys. Rev. Lett.* **93** 237004
Connétable D, Riganese G M, Charlier J C and Blase X 2005 *Phys. Rev. Lett.* **94** 015503
[31] Sapmaz S, Jarillo-Herrero P, Blanter Ya M, Dekker C and van der Zant H S J 2006 *Phys. Rev. Lett.* **96** 026801
[32] Foa Torres L E F and Roche S 2006 *Phys. Rev. Lett.* **97** 076804
[33] Foa Torres L E F and Roche S 2007 *Appl. Phys.* A **86** 283
[34] Akkermans E and Montambaux G 2004 Physique mésoscopique des électrons et des photons *EDP Sciences*
[35] McCann E, Kechedzhi K, Fal'ko Vladimir I, Suzuura H, Ando T and Altshuler B L 2006 *Phys. Rev. Lett.* **97** 146805
[36] Roche S and Mayou D 1997 *Phys. Rev. Lett.* **79** 2518
Roche S 1999 *Phys. Rev.* B **59** 2284
Roche S and Saito R 2001 *Phys. Rev. Lett.* **87** 246803
Triozon F, Roche S, Rubio A and Mayou D 2004 *Phys. Rev.* B **69** 121410
Latil S, Roche S, Mayou D and Charlier J C 2004 *Phys. Rev. Lett.* **92** 256805
Adessi Ch, Roche S and Blase X 2006 *Phys. Rev.* B **73** 125414
Avriller R, Latil S, Triozon F, Blase X and Roche S 2006 *Phys. Rev.* B **74** 121406
[37] Roche S, Jiang J, Triozon F and Saito R 2005 *Phys. Rev.* B **72** 113410
[38] Watanabe H, Kawarabayashi T, Ono Y and Ohtsuki T 2003 *J. Phys. Soc. Japan* **72** 645
Nakanishi T, Ohtsuki T and Kawarabayashi T 1997 *J. Phys. Soc. Japan* **66** 949
[39] Porezag D, Frauenheim Th and Köhler Th 1995 *Phys. Rev.* B **51** 12947
[40] Lam P K, Dacorogna M M and Cohen M L 1986 *Phys. Rev.* B **34** 5065
[41] Fisher D and Lee P A 1981 *Phys. Rev.* B **23** 6852
Kubo R 1957 *J. Phys. Soc. Japan* **12** 570
[42] Stojetz B, Mico C, Forro L and Strünk Ch 2005 *Phys. Rev. Lett.* **94** 186802
[43] Stern A, Aharonov Y and Imry Y 1990 *Phys. Rev.* A **41** 3436
See also Feynman R P and Vernon F L 2000 *Ann. Phys.* **281** 547
[44] Chakraverty S and Schmid A 1986 *Phys. Rep.* **140** 193
[45] Evensky D A, Scalettar R T and Wolynes P G 1990 *J. Phys. Chem.* **94** 1149
Nakanishi T, Ohtsuki T and Kawarabayashi T 1997 *J. Phys. Soc. Japan* **66** 949
[46] Jiang J, Saito R, Samsonidze Ge G, Chou S G, Jorio A, Dresselhaus G and Dresselhaus M S 2005 *Phys. Rev.* B **72** 235408
[47] Jiang J, Saito R, Grüneis A, Dresselhaus G and Dresselhaus M S 2004 *Chem. Phys. Lett.* **392** 383
[48] Dubay O, Kresse G and Kuzmany H 2002 *Phys. Rev. Lett.* **88** 235506
Dubay O, Kresse G and Kuzmany H 2003 *Phys. Rev.* B **67** 035401
[49] Samsonidze Ge G, Saito R, Jorio A, Pimenta M A, Souza Filho A G, Grüneis A, Dresselhaus G and Dresselhaus M S 2003 *J. Nanosci. Nanotechnol.* **3** 431
[50] Bachtold A, Fuhrer M S, Plyasunov S, Forero M, Anderson E H, Zettl A and McEuen P L 2000 *Phys. Rev. Lett.* **84** 6082

[51] Zhou X, Park J-Y, Huang S, Liu J and McEuen P L 2005 *Phys. Rev. Lett.* **95** 146805
[52] Su W P, Schrieffer J R and Heeger A J 1979 *Phys. Rev. Lett.* **42** 1698
Su W P, Schrieffer J R and Heeger A J 1980 *Phys. Rev.* B **22** 2099
[53] Lim Y S, Yee K J, Kim J H, Shaver J, Haroz E H, Kono J, Doorn S K, Hauge R H and Smalley R E 2006 *Nano Lett.* **6** 2696
[54] Shekhter R I, Gorelik L Y, Glazman L I and Jonson M 2006 *Phys. Rev. Lett.* **97** 165801
[55] Siddiqui L, Ghosh A W and Datta S 2006 *Preprint* cond-mat/0606273
[56] Mitra A, Aleiner I and Millis A J 2004 *Phys. Rev.* B **69** 245302
[57] Koch J, Semmelhack M, von Oppen F and Nitzan A 2006 *Phys. Rev.* B **73** 155306
[58] Mahan G D 2003 *Phys. Rev.* B **68** 125409
[59] Watanabe H, Kawarabayashi T and Ono Y 2005 *J. Phys. Soc. Japan* **74** 1240
[60] Anda E V, Makler S S, Pastawski H M and Barrera R G 1994 *Braz. J. Phys.* **24** 330
[61] Bonča J and Trugman S A 1995 *Phys. Rev. Lett.* **75** 2566
[62] Haule K and Bonča J 1999 *Phys. Rev.* B **59** 13087
[63] Mingo N and Makoshi K 2000 *Phys. Rev. Lett.* **84** 3694
[64] Ness H and Fisher A J 1999 *Phys. Rev. Lett.* **83** 452
[65] Emberly E G and Kirczenow G 2000 *Phys. Rev.* B **61** 5740
[66] Foa Torres L E F, Pastawski H M and Makler S S 2001 *Phys. Rev.* B **64** 193304
Pastawski H M, Foa Torres L E F and Medina E 2002 *Chem. Phys.* **281** 257
[67] Verma A, Kauser M Z and Ruden P P 2005 *J. Appl. Phys.* **97** 114319
Cazin d'Honincthun H, Gadin-Retailleau S, Sée J and Dollfus P 2005 *Appl. Phys. Lett.* **87** 171112
Koswatta S O, Hasan S, Lundstrom M S, Anantram M P and Nikonov D E 2006 *Appl. Phys. Lett.* **89** 023125